Available online at www.sciencedirect.com
SCIENCE DIRECT®
ELSEVIER
Nuclear Instruments and Methods in Physics Research B 210 (2003) 117–122
NIM B Beam Interactions with Materials & Atoms
www.elsevier.com/locate/nimb

3D imaging of elemental distributions using multi-angle RBS 2D-data

Y. Oishi [a], K. Hotta [a], K. Ishii [a,*], Y. Komori [a], S. Matsuyama [a], H. Yamazaki [a], Ts. Amartivan [a], M. Rodriguez [a], K. Katoh [a], D. Izukawa [a], K. Mizuma [a], T. Satoh [b], T. Kamiya [b], T. Sakai [b], K. Arakawa [b], M. Saidoh [b], M. Oikawa [c]

[a] *Department of Quantum Science and Energy Engineering, Tohoku University, Sendai 980-8579, Japan*
[b] *Takasaki Radiation Chemistry Research Establishment, JAERI Takasaki, Gunma 370-1292, Japan*
[c] *Ion Accelerator Corporation, Hakodate 040-0076, Japan*

Abstract

We developed a novel technique to obtain 3D-imaging of elemental distribution based on multi-angle RBS measurement and micro-beam scanning. Since cross-sections of RBS are too small to obtain 3D-imaging, it is necessary to measure scattered particles with large solid angle detectors. Hence, the RBS profiles from each scattering angle are superposed and a true depth profile cannot be obtained. Recently, a large solid angle X-ray detector array consisting of 45 detector elements was installed at the TIARA facility of Japan Energy Research Institute. Each detector element measures X-rays as well as scattered particles. For this utilization, we introduced a technique to superpose RBS profiles and applied it to the surface analysis of an ant's head.
© 2003 Elsevier B.V. All rights reserved.

PACS: 07.79.−V; 34.50.Dy
Keywords: Micro-RBS analysis; Micro-PIXE analysis; High-efficiency RBS measurement

1. Introduction

The technique to investigate the profile of elements using the energy spectrum of protons or α particles backscattered by target nuclei (RBS) is being widely used in the field of surface material physics. It is expected that 3D-images can be obtained with RBS by means of scanning beams. Recently, RBS technique combined with micro-PIXE have been applied to the analysis of mineral and industrial samples [1–5], where the samples contained very large amount of elements. Other techniques to obtain 3D-images include micro-PIXE CT [6–8] and the combination of STIM-CT [9] and micro-PIXE CT where the sample is rotated during measurement.

The peak profile of backscattered particles from light and heavy nuclei are separated in the RBS energy spectrum. Therefore, the part of RBS spectrum due to heavy elements can be distinguished from the main elements: hydrogen, carbon and oxygen in the biological samples. Moreover,

* Corresponding author. Tel./fax: +81-22-217-7931.
E-mail address: keizo.ishii@qse.tohoku.ac.jp (K. Ishii).

0168-583X/$ - see front matter © 2003 Elsevier B.V. All rights reserved.
doi:10.1016/S0168-583X(03)01080-2

3D-images can be obtained by scanning the sample with a micro-beam.

Recently, a large solid angle X-ray detection system (EURISYS MEASURES Co., Ltd.) was installed at the TIARA facility of Japan Energy Research Institute. This array of 45 X-ray detectors measures X-rays as well as scattered particles [10]. As the energy profile of backscattered particles from heavy nuclei overlap each other, they cannot be separated by RBS, however the main element yields can be determined by PIXE analysis.

In this paper, we propose a new technique to obtain the elemental profile of biological samples on the basis of RBS analysis with the multi-detector system enhanced by simultaneous PIXE analysis.

2. Proposed technique of superposing RBS spectra obtained at different measuring angles

The main components of biological samples are hydrogen, carbon, nitrogen and oxygen. The energy of particles backscattered by these light nuclei is much smaller than the RBS energy of heavy nuclei like potassium and phosphorus. Therefore, a depth profile of potassium and phosphorus in biological samples can be obtained from the high energy part of the RBS spectrum.

Table 1 shows the depth investigated by 2 MeV protons as a function of measuring angle for potassium in a protein rich biosample, which is limited by oxygen. The range of proton energies is selected considering the penetration depth of the sample and 2 MeV is adopted for the PIXE analysis. It is seen from this table that the distribution of potassium can be investigated to a depth of 7 μm at the measuring angle of 160°.

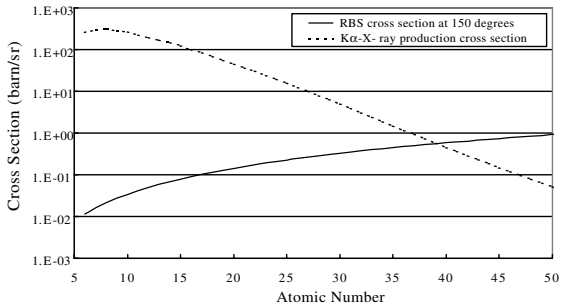

Fig. 1. RBS cross-sections at 150° and Kα X-ray production cross-sections for 2 MeV proton as a function of elemental atomic number.

Fig. 1 shows the relation between the RBS cross-sections at 150° and potassium Kα X-ray production cross-sections for 2 MeV incident protons as a function of elemental atomic numbers. As far as the cross-section is concerned, the sensitivity of RBS analysis becomes superior to that of PIXE analysis above strontium. However, in the case of heavy nuclei, the RBS energies are very close and the profiles cannot be separated. Moreover, in the case of a thick sample, their RBS profiles overlap strongly even for light elements. Since the concentration of heavy elements such as copper and iron is trace in comparison to the large amounts of phosphorus, potassium, chlorine, calcium, the contribution of those heavy elements in the RBS spectrum of the biosample is negligibly small. As a consequence one observes only the 3D-images of phosphorus and potassium here.

It is seen from Fig. 1 that the cross-section of RBS for phosphorus and potassium is two orders

Table 1
Depth investigated by 2 MeV protons as a function of measuring angle for potassium in biosample, which is limited by oxygen

Scattering angle (degrees)	Scattered energy at O surface (MeV)	Scattered energy at K surface (MeV)	Depth (μm)
120	1.655	1.851	3.91
130	1.626	1.838	4.99
140	1.601	1.826	5.89
150	1.580	1.817	6.61
160	1.566	1.810	7.14
170	1.557	1.805	7.46

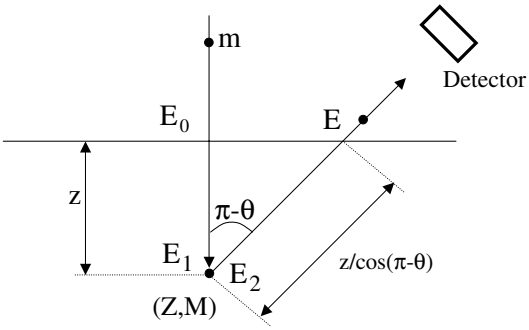

Fig. 2. Schematic diagram illustrating relation between penetrating depth z and projectile range $R(Ei)$.

of magnitude smaller than the K X-ray cross-section. Therefore one must improve the RBS count rate and the RBS measurement is thus carried out by a multi-detector array. Finally the RBS profiles are superposed.

Assuming that a small amount of a heavy element with an atomic number Z is distributed in the cytoplasm as a function $\rho(z)$ of depth z, we introduce a relation between $\rho(z)$ and the RBS energy spectrum $(\mathrm{d}N_R/\mathrm{d}E)(E,\theta)$. In Fig. 2, a projectile with incident energy E_0 and mass m passes through a sample losing a part of its energy and is subsequently backscattered by a nucleus with a atomic number Z and mass M at a position z, where the projectile energy changes kinematically from E_1 to E_2. Then, the projectile penetrates the sample and arrives at a detector in which the projectile energy E is observed. In these processes, we obtain the following relations for range $R(E)$,

$$R(E_0) = z + R(E_1), \tag{1}$$

$$R(E_2) = \frac{z}{\cos(\pi-\theta)} + R(E). \tag{2}$$

We use an empirical formula for the range $R(E)$:

$$R(E) = \alpha E^{\gamma}, \tag{3}$$

where α depends on material but γ takes a constant value ($\sim$1.75 above $E > 1$ MeV). The relation between E_1 and E_2 is given by,

$$E_2 = G(\theta)E_1, \tag{4}$$

where

$$G(\theta) = \left(\frac{\sqrt{\delta^2\cos^2\theta + 1 - \delta^2} + \delta\cos\theta}{1+\delta}\right)^2$$

and

$$\delta = \frac{m}{M}.$$

From the Eqs. (1)–(4), we obtain a relation between z and E:

$$z = \frac{\alpha(E^{\gamma} - (G(\theta)E_0)^{\gamma})}{1 - G(\theta)^{\gamma}\cos\theta}\cos\theta. \tag{5}$$

Assuming Rutherford cross-sections, the RBS energy spectrum $(\mathrm{d}N_R/\mathrm{d}E)(E,\theta)$ is presented by the equation:

$$\frac{\mathrm{d}N_R}{\mathrm{d}E}(E,\theta) = \rho(z)\frac{\mathrm{d}z}{\mathrm{d}E}N_p\frac{\mathrm{d}\sigma_R}{\mathrm{d}\Omega}\delta\Omega_D \tag{6}$$

with

$$\frac{\mathrm{d}z}{\mathrm{d}E} = \frac{\alpha\gamma E^{\gamma-1}\cos\theta}{1 - G(\theta)^{\gamma}\cos\theta}$$

and

$$\frac{\mathrm{d}\sigma_R}{\mathrm{d}\Omega} = \frac{(1+\delta^2+2\delta\cos\theta_c)^{3/2}}{|1+\delta\cos\theta_c|}\left(\frac{(1+\delta)z_pZe^2}{2(1-\cos\theta_c)E_1}\right)^2,$$

where

$$\cos\theta_c = \cos\theta\sqrt{1-\delta^2\sin^2\theta} - \delta\sin^2\theta$$

and

$$E_1 = \left(E_0^{\gamma} - \frac{z}{\alpha}\right)^{\frac{1}{\gamma}}.$$

N_p, $\delta\Omega_D$, z_p and e are the number of incident particles, detector solid angle, the atomic number of the projectile and the charge unit, respectively.

In accordance with Eqs. (5) and (6), we can derive a distribution of $\rho(z)$ for the element Z from the RBS energy spectrum $\phi(\theta,E)$. The distributions $\rho(z)$ at each angle can be superposed on each other to improve the count rate statistics.

3. Experiment and results

The experiment was carried out by using the micro-beam system and the large solid angle X-ray

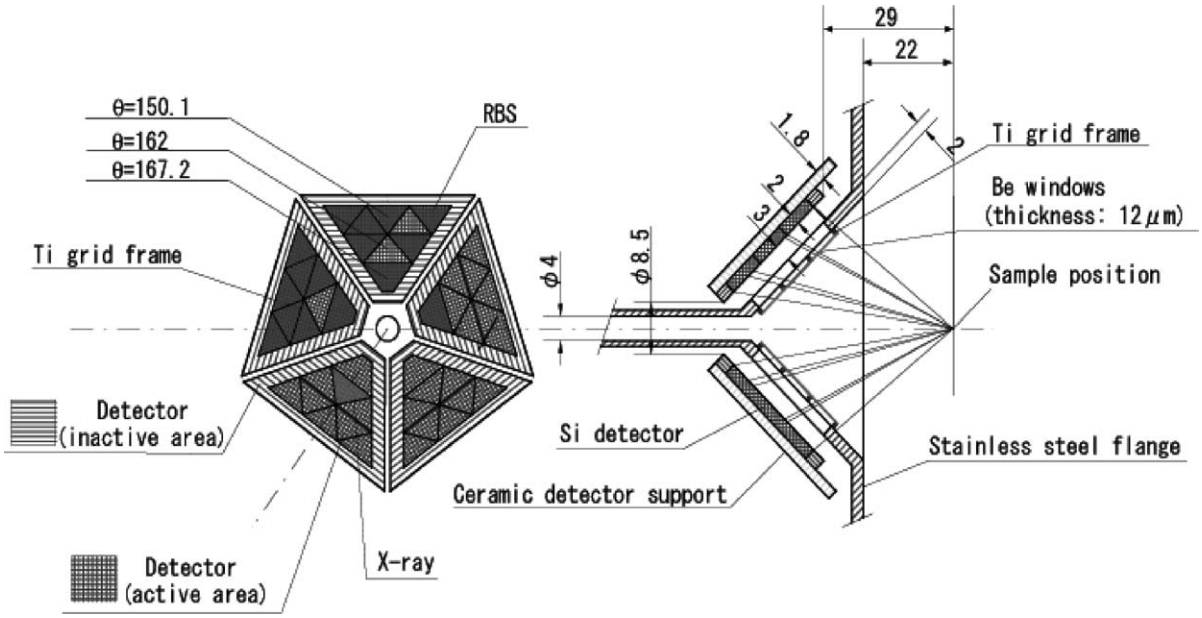

Fig. 3. Schematic diagram of the detection geometry of a large solid angle X-ray detection system.

detection system shown schematically in Fig. 3. The array consists of 45 detector elements in five elements assembled like a lamp shade in the vacuum box with 12 μm Be windows. The signals from the preamplifiers are split as input into the main amplifiers for RBS and those of PIXE. RBS signals and PIXE signals are labeled with the micro-beam position information and are stored in the computer memory. In this experiment, only 16 detectors at 148–168° were employed for RBS measurements (blue) and one detector at 150° for the PIXE measurement (orange).

Energy calibration for the detector array was carried out by RBS measurement of a 0.1 μm thick gold foil, because the RBS energy from gold nuclei only weakly depends on the scattering angle. From this calibration, we obtained an average value of energy resolution for the detectors of 3%.

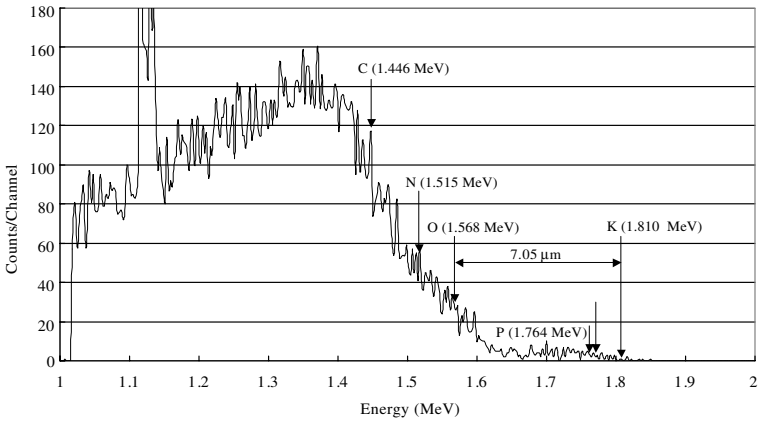

Fig. 4. RBS spectrum of the ant's head at 158.2°.

We applied our method to analyze the elemental profile of the head of a very small ant pasted with araldite to a Mylar backing. Scan area was 500 μm × 500 μm and measurements with 200 pA were carried out for 1 h using a 2 μm micro-beam. The surface of the head was defined as x–y plane and z-axis was taken in the inward direction from the surface. Fig. 4 shows the RBS spectrum at 158.2° and Fig. 5 shows the simultaneous PIXE spectrum. In these figures, the spectra are summed in the x–y plane. The contribution of RBS from heavier elements is recognized above oxygen. A composition peak of phosphorus and sulfur and the potassium peak appear strongly in the PIXE spectrum. This evidence that a combination of RBS and PIXE has considerable merits. The energy resolution of the X-ray detector was 350 eV at potassium Kα X-ray (3.313 keV).

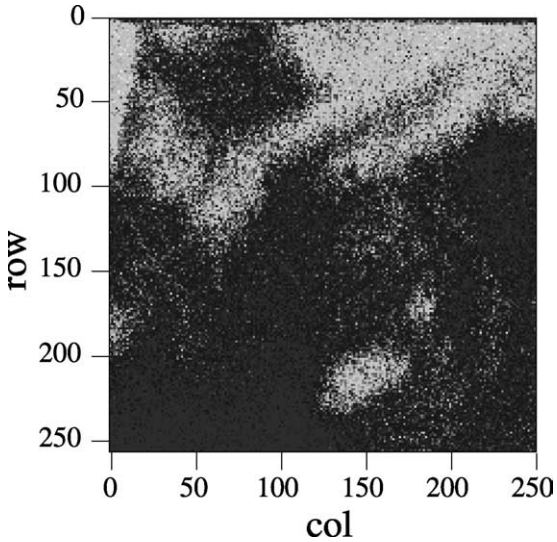

Fig. 6. 2D micro-PIXE image of phosphorus + sulfur yields.

4. Discussion and conclusion

It is seen from Fig. 5 that the contribution of phosphorus + sulfur is much larger than the one of potassium. Fig. 6 shows the 2D micro-PIXE image of phosphorus + sulfur of the ant's head. A high concentration of phosphorus or sulfur corresponds to the top of the head of ant.

Other regions of strong concentration are the contribution of sulfur contained in the araldite paste. It is thus concluded that the elemental concentration on top of the head is mainly due to phosphorus or sulfur nuclei. The energy range of RBS for phosphorus and oxygen nuclei near the surface is presented in Fig. 4. It is evident that the profile of phosphorus is obtained from the surface to a depth of slightly less than 7 μm.

Using Eqs. (5) and (6), we calculated the depth profiles from the RBS data at each angle and summed them with respect to angles. Fig. 7 shows a $2\frac{1}{2}$D-image of phosphorus + sulfur using superposed RBS data in two parts 6a(x–y plane integrated over z above oxygen) and 6b(z-axis of

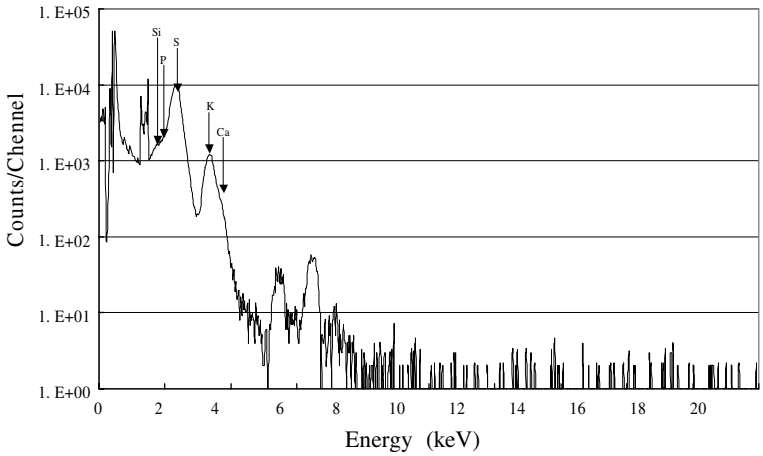

Fig. 5. PIXE spectrum of the ant's head.

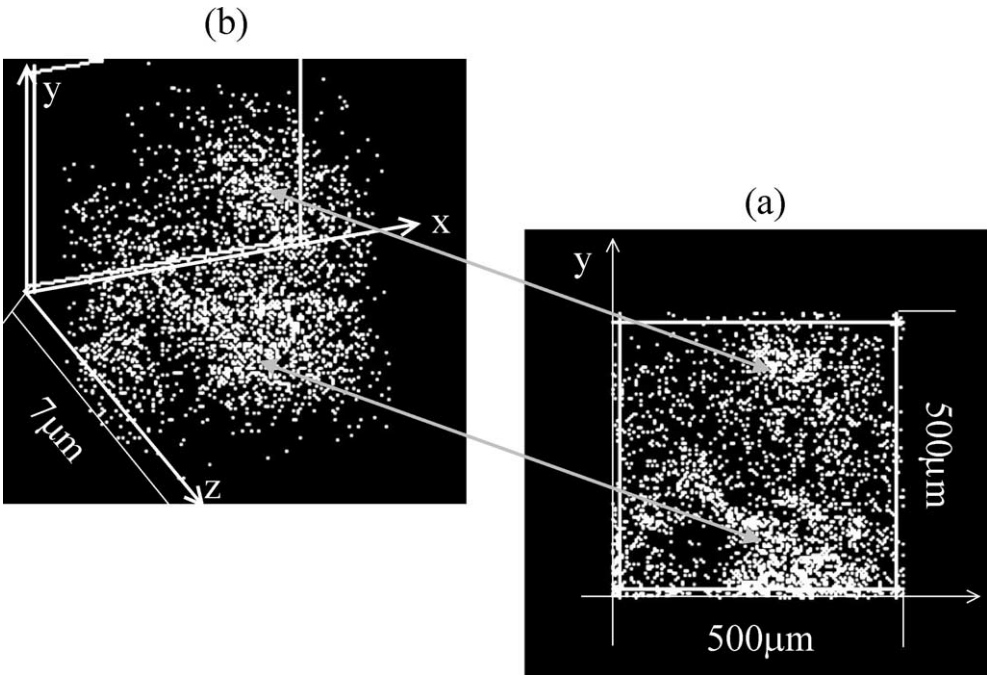

Fig. 7. $2\frac{1}{2}$D-image of phosphorus + sulfur on the surface of the ant's head using RBS data.

depth). Again it is recognized that phosphorus or sulfur is strongly enhanced at the surface of the ant's head at the upper side in Fig. 7(a). The strong concentration at the lower side in Fig. 7(a) is uniformly distributed inward from the surface and corresponds to the araldite paste. These are preliminary data but final data will have better statistics by one order of magnitude. At present the energy resolution is 60 keV resulting in a resolving power of about 1 μm in the direction of depth. By improving of energy resolution to 30 keV, the spatial resolution will be less than 1 μm.

Acknowledgement

The authors acknowledge helpful discussions with Prof. W. Galster.

References

[1] F. Watt, I. Tajta, J.A. van Kan, et al., Nucl. Instr. and Meth. B 190 (2002) 306.
[2] T. Onuki, N. Kozai, M. Samadfam, et al., Nucl. Instr. and Meth. B 181 (2001) 644.
[3] L.C. Alves, E. Alvest, G.W. Grime, et al., Nucl. Instr. and Meth. B 158 (1999) 671.
[4] A. Simon, F. Paszti, I. Uzonyi, et al., Vacuum 50 (1998) 503.
[5] J.W. McMillan, P.M. Pollard, F.C.W. Pummery, Nucl. Instr. and Meth. B 15 (1986) 394.
[6] S.C. Liew et al., Nucl. Instr. and Meth. B 104 (1995) 222.
[7] C. Michelet, Ph. Moretto, Nucl. Instr. and Meth. B 150 (1999) 173.
[8] K.A. Sjöland et al., Nucl. Instr. and Meth. B 124 (1997) 639.
[9] A. Sakellariou, D.N. Jamieson, G.J. Legge, Nucl. Instr. and Meth. B 181 (2001) 211.
[10] T. Satoh et al., Nucl. Instr. and Meth. B, submitted for publication.